Journal of Saudi Chemical Society (2015) 19, 465–470

King Saud University

Journal of Saudi Chemical Society

www.ksu.edu.sa
www.sciencedirect.com

ORIGINAL ARTICLE

The hybridization of Ag_2CO_3 rods with g-C_3N_4 sheets with improved photocatalytic activity

Konglin Wu [a,1], Yanwei Cui [a,1], Xianwen Wei [a,*], Xinjie Song [b,*], Jiarui Huang [a,c,*]

[a] *College of Chemistry and Materials Science, Center for Nano Science and Technology, Anhui Normal University, Wuhu, Anhui 241000, People's Republic of China*
[b] *Department of Food Science and Technology, Yeungnam University, Gyeongsan, Gyeongbuk 712749, Republic of Korea*
[c] *School of Chemical Engineering, Yeungnam University, Gyeongsan, Gyeongbuk 712749, Republic of Korea*

Received 27 February 2015; revised 28 June 2015; accepted 3 July 2015
Available online 10 July 2015

KEYWORDS

Ag_2CO_3;
g-C_3N_4;
Composite;
Visible-light;
Photocatalysis

Abstract A series of graphitic carbon nitride/silver carbonate (g-C_3N_4/Ag_2CO_3) rod-like composites with different weight contents of g-C_3N_4 have been prepared by a facile precipitation method. The g-C_3N_4/Ag_2CO_3 rod-like composites exhibited higher photocatalytic activity than pure Ag_2CO_3 toward degradation of rhodamine B (RhB) and methylene blue (MB) under visible-light irradiation. The photocatalytic reaction follows a pseudo-first-order reaction and the rate constants for the degradation of RhB and MB by 3.5% g-C_3N_4/Ag_2CO_3 are about 2 times and 1.7 times that of pure Ag_2CO_3, respectively. A possible photocatalytic mechanism was proposed based on the photoluminescence (PL) spectra and a series of radical trapping experimental analyses. The remarkably improved photocatalytic performance should be ascribed to the heterostructure between Ag_2CO_3 and g-C_3N_4, which greatly promoted the photoinduced charge transfer and inhibited the recombination of electrons and holes.

1. Introduction

Photocatalytic activity of the materials depends on the efficient separation of the photogenerated electrons and holes. The critical points for a good semiconductor photocatalysis are the high efficiency separation of photoexcited electron–hole pairs, the decrease of electron–hole recombination and good repeatability of photocatalysts. Recently, nanostructured materials have attracted considerable interest owing to their unique properties and potential applications [1–3]. Therefore, the decomposition of organic pollutants using various nanomaterials in the presence of sunlight has been a major topic. TiO_2 is one of the most effective photocatalysts for the degradation of organic pollutants as well as other toxic materials under

* Corresponding authors at: College of Chemistry and Materials Science, Center for Nano Science and Technology, Anhui Normal University, Wuhu, Anhui 241000, People's Republic of China (J. Huang). Tel.: +86 553 386 9301; fax: +86 553 386 9303.
E-mail addresses: xwwei@mail.ahnu.edu.cn (X. Wei), jesse.song@hotmail.com (X. Song), jrhuang@mail.ahnu.edu.cn (J. Huang).
[1] Equal contribution as the first author.

Peer review under responsibility of King Saud University.

ELSEVIER Production and hosting by Elsevier

http://dx.doi.org/10.1016/j.jscs.2015.07.002

ultraviolet (UV) light irradiation. On the other hand, TiO_2 is a wide band gap semiconductor (3.02 eV for rutile and 3.18 eV for anatase) [4], which means that it can absorb only 5% of sunlight in the UV region, limiting its practical applications. Nanocomposites can improve the visible light photocatalytic activities of wide band gap semiconductors. For example, Cho et al. developed TiO_2 nanoparticles, Au@TiO_2 and Ag@TiO_2 nanocomposites for the catalytic degradation of dyes under visible light irradiation [5–7]. Therefore, a significantly efficient, stable, inexpensive, easily separable semiconductor material that works well with visible light is a major challenge in this field [8,9].

Silver carbonate (Ag_2CO_3), a narrow band gap semiconductor, has been widely used for photocatalytic degradation of organic contaminations (e.g., rhodamine B (RhB), methylene blue (MB), methyl orange (MO) dyes and phenol) and photocatalytic destruction of *Escherichia coli* under visible-light illumination [10–12]. In general, photocatalytic activity can be improved by preparing silver-based compounds with different means, such as morphology control, size control, modification, and hybridization. More recently, graphene oxide-Ag_2CO_3 composite reported by our group showed higher visible-light photocatalytic activity than the bare Ag_2CO_3 under identical condition [13]. Here, graphene oxide used as a support can be replaced by other two dimensional materials.

In 2009, a great breakthrough was made by Wang and co-workers, who reported a new use of graphitic carbon nitride (g-C_3N_4) semiconductor, which can produce hydrogen from water under visible-light irradiation [14]. After that, numerous g-C_3N_4/silver-based semiconductor hybrid photocatalysts have been extensively reported, such as the composites of g-C_3N_4/Ag_3VO_4 [15], g-C_3N_4/Ag_3PO_4 [16], g-C_3N_4/Ag_2O [17], and g-C_3N_4/Ag_2CO_3 composites [18–21]. The g-C_3N_4 partly modified with Ag_3VO_4, Ag_3PO_4, Ag_2O, and Ag_2CO_3 exhibited remarkably enhanced photocatalytic performances. Herein, a facile precipitation method was developed to prepare a series of g-C_3N_4/Ag_2CO_3 rod-like composites for the first time. Compared with the pure Ag_2CO_3, the novel g-C_3N_4/Ag_2CO_3 hybrid photocatalysts possessed higher photocatalytic activity toward the degradation of RhB and MB under visible-light irradiation.

2. Experimental section

2.1. Synthesis of g-C_3N_4

The g-C_3N_4 powder was synthesized according to the literature [22]. Typically, 10 g of melamine was put into an alumina crucible with a cover and heated at a rate of 20 °C min^{-1} to 550 °C in a muffle furnace and then kept at this temperature for 4 h. All the experiments were performed under air conditions. The resulting yellow product was collected and ground into powder for further use.

2.2. Synthesis of g-C_3N_4/Ag_2CO_3 composites

Typically, 20 mL g-C_3N_4 dispersions with different concentrations (0.1, 0.25, 0.35, 0.5 and 1 mg/mL) were treated with ultrasonic for 2 h, then 5 mL aqueous solution of $AgNO_3$ (0.2 M) was added under magnetic stirring, and then kept stirring for another 1 h in the dark. At last, 5 mL aqueous solution of $NaHCO_3$ (0.1 M) was added dropwise into the above mixture under magnetic stirring, and then kept stirring for additional 12 h in the dark. The final products were collected by centrifugation, washed with de-ionized water and absolute ethanol several times and dried in vacuum at room temperature for 24 h. For convenience, the as-prepared composites with different weight contents of g-C_3N_4 were labeled by 1.4% g-C_3N_4/Ag_2CO_3, 3.5% g-C_3N_4/Ag_2CO_3, 4.8% g-C_3N_4/Ag_2CO_3, 6.8% g-C_3N_4/Ag_2CO_3 and 12.7% g-C_3N_4/Ag_2CO_3, respectively. The pure Ag_2CO_3 was synthesized via a parallel process but without g-C_3N_4.

2.3. Characterization

Structure and morphology of the products were characterized by X-ray powder diffraction (XRD, Philips X'Pert PRO), scanning electron microscopy (SEM, Hitachi S-4800), and high-resolution transmission electron microscopy (TEM, JEOL-2010 TEM with an acceleration voltage of 200 kV), respectively. UV–visible diffuse reflectance spectra (DRS) were recorded by a Shimadzu UV-2450 spectrometer using MgO (light) as a standard at room temperature. The photoluminescence (PL) spectra for solid samples dispersed in absolute ethanol were investigated with an excitation wavelength of 320 nm on a Hitachi F-4500 fluorescence spectrophotometer.

2.4. Photocatalytic evaluation

The optical system for the photocatalytic reaction was composed of a 500 W Xe lamp (Shanghai Jiguang Special Light, China) and a cutoff filter ($\lambda > 400$ nm). RhB or MB aqueous solution (30 mL, 10 mg/L) containing 20 mg of catalyst was put in a sealed glass beaker and first ultrasonicated for several minutes, and then stirred in the dark for 1 h to ensure absorption–desorption equilibrium. After visible-light illumination at regular time intervals, the absorbance of dye solution was monitored by a Hitachi U-3010 UV–vis spectrophotometer.

3. Results and discussion

The structure information of the as-prepared products was collected by XRD. Fig. 1(I) shows a typical XRD pattern of pure Ag_2CO_3. All the diffraction peaks can be well-indexed to a monoclinic crystalline phase Ag_2CO_3 (JCPDS No. 12-0766). The XRD pattern of pure g-C_3N_4 is displayed in Fig. 1(VII), the strongest peak at 27.5° corresponding to the (0 0 2) plane arising from the stacking of the conjugated aromatic system and the other peak at 13.1° corresponding to the (1 0 0) plane are associated with interlayer stacking [16–18]. We also found that the XRD patterns of g-C_3N_4/Ag_2CO_3 composites were similar to those of pure Ag_2CO_3 (Fig. 1(II)–(IV)), but with the increasing weight contents of g-C_3N_4, the characteristic peak of g-C_3N_4 gradually appears (Fig. 1(V) and (VI)). Therefore, the formation of g-C_3N_4/Ag_2CO_3 composites has been proved.

The morphology of the products was studied by SEM. Fig. 2(a) shows a SEM image of pure Ag_2CO_3, which was composed of straight and smooth rod with ca. 500 nm in diameter and 2 μm in length. The SEM image of g-C_3N_4 sheets is also given in Fig. S1 (see ESI). From Fig. 2(b)–(f), we can

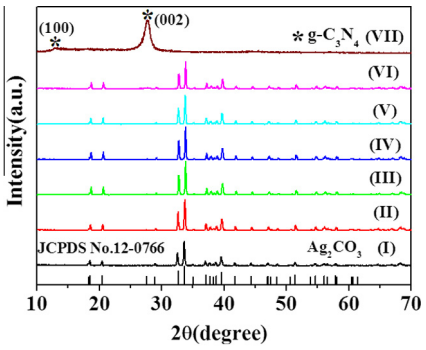

Figure 1 XRD patterns of (I) Ag_2CO_3, (II) 1.4% g-C_3N_4/Ag_2CO_3, (III) 3.5% g-C_3N_4/Ag_2CO_3, (IV) 4.8% g-C_3N_4/Ag_2CO_3, (V) 6.8% g-C_3N_4/Ag_2CO_3, (VI) 12.7% g-C_3N_4/Ag_2CO_3, and (VII) g-C_3N_4.

see that Ag_2CO_3 rods are randomly deposited on the g-C_3N_4 sheets. We believe that the hybridization of Ag_2CO_3 with g-C_3N_4 is beneficial to the synergistic interaction between Ag_2CO_3 rods and g-C_3N_4 sheets. The morphology of the g-C_3N_4/Ag_2CO_3 composite was also investigated by TEM. Fig. S2 (see ESI) shows the TEM images of the 3.5% g-C_3N_4/Ag_2CO_3 sample. From the TEM image of g-C_3N_4/Ag_2CO_3 sample, it can be seen that g-C_3N_4 was successfully dispersed on the surface of Ag_2CO_3 and the heterostructure between g-C_3N_4 and Ag_2CO_3 was formed in the g-C_3N_4/Ag_2CO_3 composite.

The optical absorbance of the as-obtained samples was measured by UV–vis diffuse reflectance spectroscopy (Fig. S3(a)). The absorption spectrum of Ag_2CO_3 extends from UV to visible region (480 nm). After being modified by g-C_3N_4, the color of the g-C_3N_4/Ag_2CO_3 composites changed from dark yellow to bright yellow (inset Fig. S3(a)) and there is an enhanced absorbance in the visible-light region ranging from 480 to 800 nm. Fig. S3(b) shows the plots of the transformed Kubelka–Munk function of light energy $(\alpha h\nu)^{1/2}$ versus energy ($h\nu$) for the as-prepared samples. Ag_2CO_3 belongs to indirect band gap semiconductor and its band gap is estimated to be 2.34 eV, which is close to the values in the previous reports [10–12]. The band gaps of g-C_3N_4/Ag_2CO_3 composites are also calculated to be 2.18, 2.12, 2.17, 2.23, 2.29 eV, respectively, as displayed in Table 1. This indicates a band gap narrowing of the semiconductor Ag_2CO_3 due to the introduction of g-C_3N_4 into the matrix of Ag_2CO_3, which can be attributed to the synergistic interaction between semiconductor and g-C_3N_4 support. Furthermore, the absorption edge of the pure g-C_3N_4 is at about 470 nm, which originates from its band gap

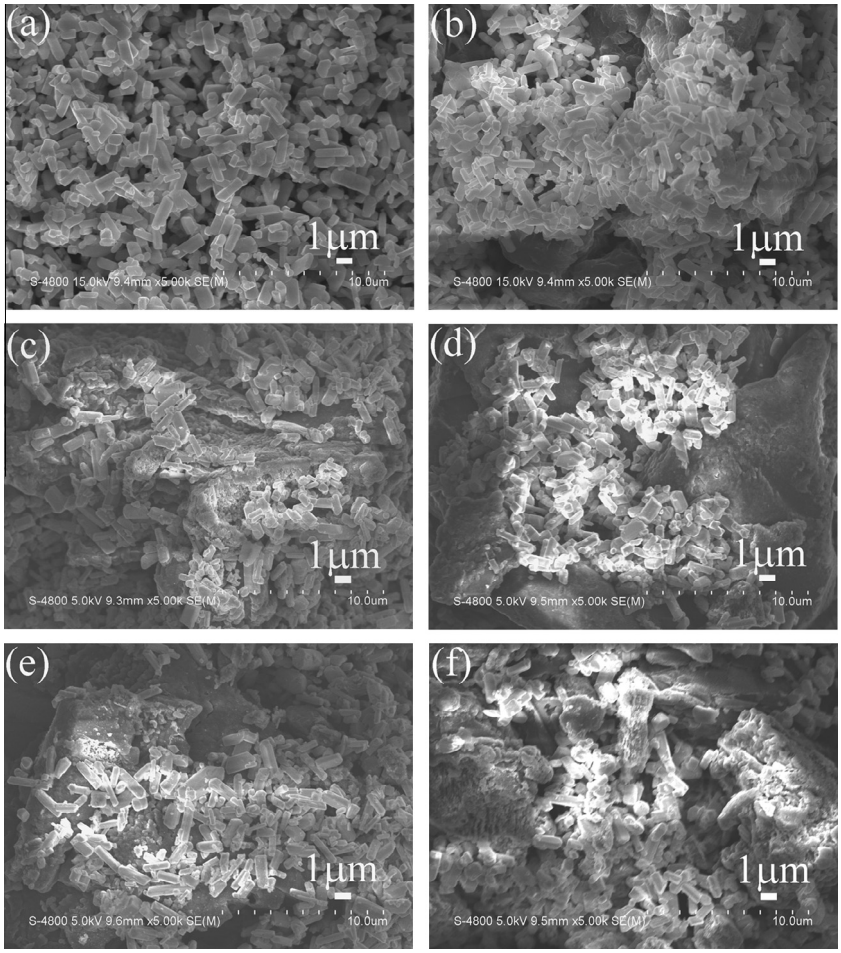

Figure 2 SEM images of (a) Ag_2CO_3, (b) 1.4% g-C_3N_4/Ag_2CO_3, (c) 3.5% g-C_3N_4/Ag_2CO_3, (d) 4.8% g-C_3N_4/Ag_2CO_3, (e) 6.8% g-C_3N_4/Ag_2CO_3, and (f) 12.7% g-C_3N_4/Ag_2CO_3.

Table 1 The band gaps (Eg) and first-order rate constants (k) of the as-prepared samples.

Samples	Eg (eV)	k (min^{-1})	
		RhB	MB
Ag_2CO_3	2.34	0.04413	0.06703
1.4% g-C_3N_4/Ag_2CO_3	2.18	0.05675	0.06968
3.5% g-C_3N_4/Ag_2CO_3	2.12	0.08603	0.11112
4.8% g-C_3N_4/Ag_2CO_3	2.17	0.07328	0.09177
6.8% g-C_3N_4/Ag_2CO_3	2.23	0.04144	0.04941
12.7% g-C_3N_4/Ag_2CO_3	2.29	0.03058	0.02871
g-C_3N_4	2.63	0.00579	0.00722

of ~2.63 eV and is consistent with the reported results [16,17,22].

The photocatalytic performance of Ag_2CO_3, g-C_3N_4/Ag_2CO_3 composites and g-C_3N_4 is evaluated by the degradation of RhB and MB under visible-light irradiation. As shown in Figs. 3, S4 and S5, the degradation efficiency of RhB and MB follows the order 3.5% g-C_3N_4/Ag_2CO_3 > 4.8% g-C_3N_4/Ag_2CO_3 > 1.4% g-C_3N_4/Ag_2CO_3 > Ag_2CO_3 > 6.8% g-C_3N_4/Ag_2CO_3 > 12.7% g-C_3N_4/Ag_2CO_3 > g-C_3N_4. Obviously, the addition of an appropriate amount of g-C_3N_4 can enhance the photocatalytic activity effectively. However, superfluous g-C_3N_4 will decrease photocatalytic performance, indicating a synergistic interaction between g-C_3N_4 sheets and Ag_2CO_3 rods is required in order to improve the photoactivity of semiconductor Ag_2CO_3 rods. The optimal weight content of g-C_3N_4 in this study is 3.5%. Assuming that the photocatalytic reaction follows a pseudo-first-order reaction due to low concentration of the dye solutions, the relevant equations are listed as follows: $-\ln(C_t/C_0) = kt$, where C_0 and C_t are the concentrations of reactant at time 0 and t, respectively, and k is the first-order reaction rate constant [23,24]. The corresponding first-order rate constants are shown in Fig. S6 and listed in Table 1. It is noted that the degradation rate constants for MB by g-C_3N_4/Ag_2CO_3 composites are higher than those for RhB on the general trend, which indicates that MB is more easily degraded under the same conditions. Significantly, the first-order rate constants for the degradation of RhB and MB by 3.5% g-C_3N_4/Ag_2CO_3 are 0.08603 and 0.11112 min^{-1}, respectively, which are about 2 times and 1.7 times that of pure Ag_2CO_3 (0.04413 and 0.06703 min^{-1}).

As is known to all, the behavior of photogenerated charge carriers is a key factor to determine the performance of photocatalysts [25]. The separation and lifetime of photogenerated electron–hole pairs can be confirmed by the PL spectra. The PL intensity with higher value means more recombination of electron–hole pairs and lower photocatalytic activity [15]. As displayed in Fig. S7, under excitation wavelength of 320 nm, for g-C_3N_4 sheets, a strong emission peak at about 465 nm is detected. The PL peak intensity of 3.5% g-C_3N_4/Ag_2CO_3 composite is close to pure Ag_2CO_3, but dramatically decreases compared with g-C_3N_4. However, the band gap of 3.5% g-C_3N_4/Ag_2CO_3 composite is narrower than Ag_2CO_3 as well as g-C_3N_4, leading to a more light harvest, thus further improving its photoactivity. As a result, both the band gap of photocatalyst and the separation of electron–hole pairs have an influence on the performance of the photocatalyst.

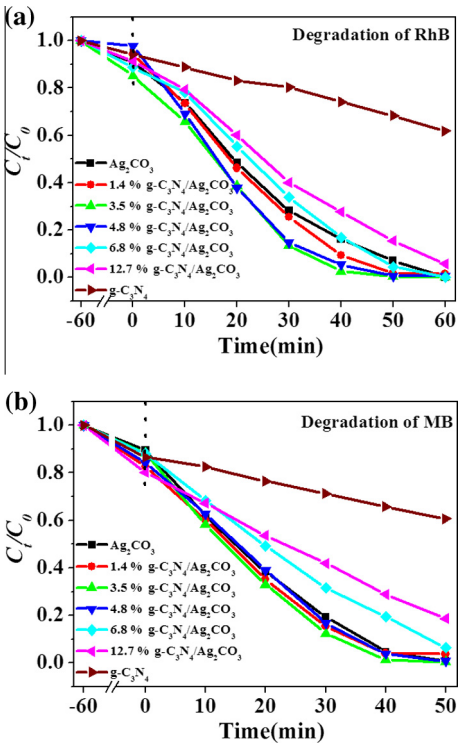

Figure 3 Photocatalytic activities of as-prepared photocatalysts for degradation of (a) RhB and (b) MB under visible-light irradiation.

In the photodegradation process, some active species including holes (h^+), hydroxyl radicals ($^{\cdot}OH$) and superoxide radicals ($^{\cdot}O_2^-$) were formed by light irradiation. $^{\cdot}O_2^-$ was formed by direct reduction of O_2 with electron [19,21]. The $^{\cdot}OH$ was obtained by the direct hole oxidation or photogenerated electron induced multistep reductions of $^{\cdot}O_2^-$. Furthermore, holes could directly react with organic compounds if the photocatalyst has moderate redox potential. Therefore, in order to understand the interaction between Ag_2CO_3 and g-C_3N_4, the active species generated during the photodegradation process over g-C_3N_4, Ag_2CO_3 and g-C_3N_4/Ag_2CO_3 can be identified by active species scavenging experiments. In the previous report, the trapping experiments of free radicals and holes were carried out by Li etc. to investigate the main reactive species for degradation of MO and RhB by g-C_3N_4/Ag_2CO_3 composite [21]. They found that the degradation rate of MO decelerated obviously after the addition of disodium ethylenediaminetetraacetate (EDTA) or 1,4-benzoquinone (BQ). However, the degradation rate showed almost no change in the presence of tert-butyl alcohol (t-BuOH), suggesting that the holes and $^{\cdot}O_2^-$ are the main reactive species for degradation of MO. For the degradation of RhB, the photocatalytic activity decreased slightly after the addition of t-BuOH. However, it is inhibited greatly in the presence of EDTA and BQ, indicating that the holes and $^{\cdot}O_2^-$ also play a major role in the degradation of RhB [19–21].

Based on the above analyses and the related literature reports, the possible mechanism of the enhanced photocatalytic activity of the g-C_3N_4/Ag_2CO_3 composites was proposed and shown in Fig. 4. Under visible light irradiation, both g-C_3N_4 and Ag_2CO_3 could absorb visible light and were all

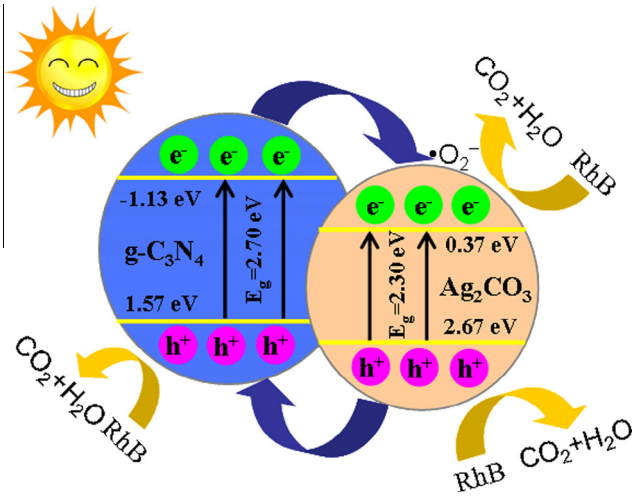

Figure 4 Band structure diagram and electron–hole separation of g-C_3N_4/Ag_2CO_3 composite.

excited to generate electron and hole pairs. The holes on the surfaces of g-C_3N_4 and Ag_2CO_3 could directly decompose the RhB molecules into the intermediates. g-C_3N_4 has a more negative potential of the conduction band (CB) and valence band (VB) than that of Ag_2CO_3. Therefore, the excited electrons on g-C_3N_4 could directly be injected into the CB of Ag_2CO_3, meanwhile the holes could migrate from the VB of Ag_2CO_3 to that of g-C_3N_4, which promotes the effective separation of photoexcited electrons and holes. As a result, the enriched electrons on the CB of Ag_2CO_3 will react with oxygen to generate $\cdot O_2^-$. The $\cdot O_2^-$ active species together with the holes on the VB of g-C_3N_4 are responsible for the degradation of organic pollutants.

The stability and reusability of catalysts are very important issues for practical applications. The g-C_3N_4/Ag_2CO_3 composite could be readily recycled by simple centrifugation after reaction. The stability and reusability of the 3.5% g-C_3N_4/Ag_2CO_3 composite were examined by repetitive use of the catalyst. As shown in Fig. S8 (see ESI), the catalyst exhibited a little loss of activity after three photodegradation cycles of RhB. However, it still kept high photocatalytic activity after three photodegradation cycles of RhB, indicating its excellent stability and great potential value in environmental purification. g-C_3N_4 possesses a conjugated π structure, which has been proven to effectively suppress photocorrosion during the g-C_3N_4 based photocatalytic reaction [26].

The photocatalyst after the reusability experiments was further analyzed by SEM and XRD to study the photostability of 3.5% g-C_3N_4/Ag_2CO_3 composite. The SEM image of the spent sample (Fig. S9, see ESI) was found to be the same morphologies as those of the fresh sample. Fig. S10 (see ESI) shows the XRD patterns of 3.5% g-C_3N_4/Ag_2CO_3 composite before and after degradation of RhB. After three catalytic runs, the peak positions had no obvious changes. However, the XRD analysis of the sample (three cycling runs) indicated that the intensity of recycled 3.5% g-C_3N_4/Ag_2CO_3 sample decreased and the diffraction peak at 2θ values 38.1° was assigned to the (1 1 1) lattice plane of Ag nanoparticles [18,19,27,28]. In order to further confirm the existence of Ag after the photodegradation, Shi etc. checked the spent g-C_3N_4/Ag_2CO_3 composite by X-ray photoelectron spectroscopy (XPS). Compared with the fresh g-C_3N_4/Ag_2CO_3 composite, Ag 3d peak showed a larger full width at half maximum. And Ag $3d_{5/2}$ and $3d_{3/2}$ peak could be further divided into two different peaks. The peaks at 368.9 and 374.8 eV were assigned to metallic Ag (0). The results suggested that partial Ag_2CO_3 was reduced to Ag in the process of photocatalytic reaction [19,21]. So during the photocatalytic reaction, the g-C_3N_4/Ag_2CO_3 system was transformed to be g-C_3N_4/Ag/Ag_2CO_3 system. There are two reasons to explain the decreasing photocatalytic activity of the g-C_3N_4/Ag_2CO_3 composite after three cycling runs. One reason is that the Ag nanoparticles gradually formed on the Ag_2CO_3 surface under the photocatalytic reaction process, which prevents the light absorption of Ag_2CO_3. Another reason is that the formed Ag nanoparticles also serve as the capture center of the electrons and holes.

4. Conclusions

In summary, we have developed a simple precipitation method for the preparation of g-C_3N_4/Ag_2CO_3 composites with different weight contents of g-C_3N_4. The 3.5% g-C_3N_4/Ag_2CO_3 photocatalyst exhibited higher photocatalytic activity for RhB and MB degradation under visible light irradiation than bare Ag_2CO_3 rods. The enhanced photocatalytic activity should be attributed to the efficient separation of photoinduced charge carriers resulted from effective fabrication of g-C_3N_4/Ag_2CO_3 heterojunction, as confirmed by the PL spectra. This work might provide a simple and high-efficient approach for removal of organic pollutants by using solar energy.

Acknowledgements

This work is supported financially by the National Natural Science Foundation (Nos. 21071005, 21271006) of P. R. China, the Research Culture Funds (Nos. 2011rcpy038, 2014xmpy13), the Innovation Funds (No. 2014cxjj13), and the Undergraduate Innovation Training Plans (Nos. 201410370198, 201410370199) of Anhui Normal University.

Appendix A. Supplementary data

Supplementary data associated with this article can be found, in the online version, at http://dx.doi.org/10.1016/j.jscs.2015.07.002.

References

[1] J.R. Huang, H.B. Ren, K.K. Chen, J.J. Shim, Controlled synthesis of porous Co_3O_4 micro/nanostructures and their photocatalysis property, Superlattices Microstruct. 75 (2014) 843–856.
[2] J.R. Huang, G.J. Fu, C.C. Shi, X.Y. Wang, M.H. Zhai, C.P. Gu, Novel porous CuO microrods: synthesis, characterization, and their photocatalysis property, J. Phys. Chem. Solids 75 (2014) 1011–1016.
[3] J.R. Huang, H.B. Ren, P.P. Sun, C.P. Gu, Y.F. Sun, J.H. Liu, Facile synthesis of porous ZnO nanowires consisting of ordered nanocrystallites and their enhanced gas-sensing property, Sens. Actuator B-Chem. 188 (2013) 249–256.

[4] S.H. Xu, W.F. Shangguan, J. Yuan, J.W. Shi, M.X. Chen, Photocatalytic properties of bismuth titanate $Bi_{12}TiO_{20}$ prepared by co-precipitation processing, Mater. Sci. Eng. B 137 (2007) 108–111.
[5] M.M. Khan, S.A. Ansari, D. Pradhan, M.O. Ansari, D.H. Han, J. Lee, M.H. Cho, Band gap engineered TiO_2 nanoparticles for visible light induced photoelectrochemical and photocatalytic studies, J. Mater. Chem. A 2 (2014) 637–644.
[6] M.M. Khan, J. Lee, M.H. Cho, Au@TiO_2 nanocomposites for the catalytic degradation of methyl orange and methylene blue: an electron relay effect, J. Ind. Eng. Chem. 20 (2014) 1584–1590.
[7] M.M. Khan, S.A. Ansari, M.I. Amal, J. Lee, M.H. Cho, Highly visible light active Ag@TiO_2 nanocomposites synthesized using an electrochemically active biofilm: a novel biogenic approach, Nanoscale 5 (2013) 4427–4435.
[8] S. Kumar, T. Surendar, B. Kumar, A. Baruah, V. Shanker, Synthesis of a novel and stable g-C_3N_4–Ag_3PO_4 hybrid nanocomposite photocatalyst and study of the photocatalytic activity under visible light irradiation, J. Mater. Chem. A 1 (2013) 5333–5340.
[9] J. Fu, B.B. Chang, Y.L. Tian, F.N. Xi, X.P. Dong, Novel C_3N_4–CdS composite photocatalysts with organic–inorganic heterojunctions: in situ synthesis, exceptional activity, high stability and photocatalytic mechanism, J. Mater. Chem. A 1 (2013) 3083–3090.
[10] C.W. Xu, Y.Y. Liu, B.B. Huang, H. Li, X.Y. Qin, X.Y. Zhang, Y. Dai, Preparation, characterization, and photocatalytic properties of silver carbonate, Appl. Surf. Sci. 257 (2011) 8732–8736.
[11] G.P. Dai, J.G. Yu, G. Liu, A new approach for photocorrosion inhibition of Ag_2CO_3 photocatalyst with highly visible-light-responsive reactivity, J. Phys. Chem. C 116 (2012) 15519–15524.
[12] H.J. Dong, G. Chen, J.X. Sun, C.M. Li, Y.G. Yu, D.H. Chen, A novel high-efficiency visible-light sensitive Ag_2CO_3 photocatalyst with universal photodegradation performances: simple synthesis, reaction mechanism and first-principles study, Appl. Catal. B: Environ. 134–135 (2013) 46–54.
[13] C. Dong, K.L. Wu, X.W. Wei, X.Z. Li, L. Liu, T.H. Ding, J. Wang, Y. Ye, Synthesis of graphene oxide–Ag_2CO_3 composites with improved photoactivity and anti-photocorrosion, CrystEngComm 16 (2014) 730–736.
[14] X.C. Wang, K. Maeda, A. Thomas, K. Takanabe, G. Xin, J.M. Carlsson, K. Domen, M. Antonietti, A metal-free polymeric photocatalyst for hydrogen production from water under visible light, Nat. Mater. 8 (2009) 76–80.
[15] S.M. Wang, D.L. Li, C. Sun, S.G. Yang, Y. Guan, H. He, Synthesis and characterization of g-C_3N_4/Ag_3VO_4 composites with significantly enhanced visible-light photocatalytic activity for triphenylmethane dye degradation, Appl. Catal. B: Environ. 144 (2014) 885–892.
[16] P.Z. He, L.M. Song, S.J. Zhang, X.Q. Wu, Q.W. Wei, Synthesis of g-C_3N_4/Ag_3PO_4 heterojunction with enhanced photocatalytic performance, Mater. Res. Bull. 51 (2014) 432–437.
[17] M. Xu, L. Han, S.J. Dong, Facile fabrication of highly efficient g-C_3N_4/Ag_2O heterostructured photocatalysts with enhanced visible-light photocatalytic activity, ACS Appl. Mater. Interfaces 5 (2013) 12533–12540.
[18] H. Xu, Y.X. Song, Y.H. Song, J.X. Zhu, T.T. Zhu, C.B. Liu, D.X. Zhao, Q. Zhang, H.M. Li, Synthesis, characterization of g-C_3N_4/Ag_2CO_3 with enhanced visible-light photocatalytic activity for the degradation of organic pollutants, RSC Adv. 4 (2014) 34539–34547.
[19] L. Shi, L. Liang, F.X. Wang, M.S. Liu, J.M. Sun, Enhanced visible-light photocatalytic activity and stability over g-C_3N_4/Ag_2CO_3 composites, J. Mater. Sci. 50 (2015) 1718–1727.
[20] N. Tian, H.W. Huang, Y. He, Y.X. Guo, Y.H. Zhang, Organic–inorganic hybrid photocatalyst g-C_3N_4/Ag_2CO_3 with highly efficient visible-light-active photocatalytic activity, Colloids Surf. A: Physicochem. Eng. Aspects 467 (2015) 188–194.
[21] Y.F. Li, L. Fang, R.X. Jin, Y. Yang, X. Fang, Y. Xing, S.Y. Song, Preparation and enhanced visible light photocatalytic activity of novel g-C_3N_4 nanosheets loaded with Ag_2CO_3 nanoparticles, Nanoscale 7 (2015) 758–764.
[22] S.C. Yan, Z.S. Li, Z.G. Zou, Photodegradation performance of g-C_3N_4 fabricated by directly heating melamine, Langmuir 25 (2009) 10397–10401.
[23] P.Y. Dong, Y.Y. Wang, B.C. Cao, S.Y. Xin, L.N. Guo, F.H. Li, Ag_3PO_4/reduced graphite oxide sheets nanocomposites with highly enhanced visible light photocatalytic activity and stability, Appl. Catal. B: Environ. 132–133 (2013) 45–53.
[24] V.A. Sakkas, I.M. Arabatzis, I.K. Konstantinou, A.D. Dimou, T.A. Albanis, P. Falaras, Metolachlor photocatalytic degradation using TiO_2 photocatalysts, Appl. Catal. B: Environ. 49 (2004) 195–205.
[25] L. Han, P. Wang, S.J. Dong, Progress in graphene-based photoactive nanocomposites as a promising class of photocatalyst, Nanoscale 4 (2012) 5814–5825.
[26] S. Kumar, T. Surendar, A. Baruah, V. Shanker, Synthesis of a novel and stable g-C_3N_4–Ag_3PO_4 hybrid nanocomposite photocatalyst and study of the photocatalytic activity under visible light irradiation, J. Mater. Chem. A 1 (2013) 5333–5340.
[27] B.Z. Tian, R.F. Dong, J.M. Zhang, S.Y. Bao, F. Yang, J.L. Zhang, Sandwich-structured AgCl@Ag@TiO_2 with excellent visible-light photocatalytic activity for organic pollutant degradation and *E. coli* K12 inactivation, Appl. Catal. B: Environ. 158–159 (2014) 76–84.
[28] Y.X. Yang, W. Guo, Y.N. Guo, Y.H. Zhao, X. Yuan, Y.H. Guo, Fabrication of Z-scheme plasmonic photocatalyst Ag@AgBr/g-C_3N_4 with enhanced visible-light photocatalytic activity, J. Hazard. Mater. 271 (2014) 150–159.